



2014

Energy-efficient magnetoelastic non-volatile memory

Ayan K. Biswas

Virginia Commonwealth University, biswasak@vcu.edu

Supriyo Bandyopadhyay

Virginia Commonwealth University, sbandy@vcu.edu

Jayasimha Atulasimha

Virginia Commonwealth University, jatulasimha@vcu.edu

Follow this and additional works at: http://scholarscompass.vcu.edu/egre_pubs

 Part of the [Electrical and Computer Engineering Commons](#)

Biswas, A.K., Bandyopadhyay, S., Atulasimha, J. Energy-efficient magnetoelastic non-volatile memory. *Applied Physics Letters*, 104, 232403 (2014). Copyright © 2014 AIP Publishing LLC.

Downloaded from

http://scholarscompass.vcu.edu/egre_pubs/13

This Article is brought to you for free and open access by the Dept. of Electrical and Computer Engineering at VCU Scholars Compass. It has been accepted for inclusion in Electrical and Computer Engineering Publications by an authorized administrator of VCU Scholars Compass. For more information, please contact libcompass@vcu.edu.

Energy-efficient magnetoelastic non-volatile memory

Ayan K. Biswas,¹ Supriyo Bandyopadhyay,¹ and Jayasimha Atulasimha²

¹Department of Electrical and Computer Engineering, Virginia Commonwealth University, Richmond, Virginia 23284, USA

²Department of Mechanical and Nuclear Engineering, Virginia Commonwealth University, Richmond, Virginia 23284, USA

(Received 20 February 2014; accepted 28 May 2014; published online 10 June 2014)

We propose an improved scheme for low-power writing of binary bits in non-volatile (multiferroic) magnetic memory with electrically generated mechanical stress. Compared to an earlier idea [N. Tiercelin *et al.*, J. Appl. Phys. **109**, 07D726 (2011)], our scheme improves distinguishability between the stored bits when the latter are read with magneto-tunneling junctions. More importantly, the write energy dissipation and write error rate are reduced significantly if the writing speed is kept the same. Such a scheme could be one of the most energy-efficient approaches to writing bits in magnetic non-volatile memory. © 2014 AIP Publishing LLC. [<http://dx.doi.org/10.1063/1.4882276>]

There is an ongoing quest to find energy-efficient strategies for writing binary bits in non-volatile magnetic memory. Writing requires rotating the magnetization of a shape-anisotropic nanomagnet between its two stable orientations that encode the bits “0” and “1.” This can be achieved with either a magnetic field generated by an electrical current,¹ or a spin transfer torque (STT) arising from a spin-polarized current,² or domain wall motion induced by a spin-polarized current.³ However, a much more energy-efficient approach is to rotate the magnetization of a two-phase multiferroic elliptical nanomagnet, comprising a magnetostrictive layer in elastic contact with a piezoelectric layer, with uniaxial mechanical stress generated by applying an electrical voltage across the piezoelectric layer.^{4–6} Normally, the maximum rotation possible with such a magneto-elastic scheme is 90°, unless the stress (or voltage) is withdrawn at precisely the right juncture to allow the magnetization to rotate further to 180°. Such precise withdrawal is a challenge, which is why complete bit flips are difficult to achieve. As a result, magneto-elastic switching has not been the preferred method to write bits in non-volatile memory, despite its vastly superior energy-efficiency.

Recently, this impasse was overcome with a clever scheme.^{8–10} A small in-plane magnetic field is applied along the minor axis of the elliptical magnetostrictive nanomagnet to move the stable magnetization directions away from the major axis to two mutually perpendicular in-plane directions that lie between the major and minor axes. They encode the bits “0” and “1.” Uniaxial stress is applied along (or close to) one of these stable directions (say, the one representing bit “0”) by applying an in-plane electric field between two electrodes delineated on the piezoelectric layer (see Fig. 1 of Ref. 9). This field generates strain in the piezoelectric layer via the d_{33} coupling, a part of which is transferred to the magnetostrictive magnet. If the magnet has a positive magnetostriction coefficient, then tensile stress will rotate the magnetization close to the direction of applied stress (or electric field) since that orientation will be the global energy minimum. Compressive stress will rotate it nearly perpendicular to the direction of applied stress, i.e., close to the other stable direction, since that will become the global energy

minimum. The situation will be the opposite if the magnetostriction coefficient is negative, but that case is completely equivalent to the first and hence is not discussed separately. When stress is finally withdrawn, the rotated magnetization will move to the stable direction closer to the stress-axis, with $\sim 100\%$ probability, and remain there in perpetuity, since that will be energetically favored. Therefore, tensile stress (voltage of one polarity) can be used to write the bit “0” and compressive stress (voltage of the other polarity) can write the bit “1.” This allows nearly error-free deterministic writing of bits, irrespective of what the originally stored bit was. A similar idea utilizing 4-state magnets was discussed earlier by Pertsev and Kohlstedt.¹¹

The disadvantage of this scheme is that it restricts the angle between the two stable magnetization orientations to $\sim 90^\circ$. The stored bit is usually read with a magneto-tunneling junction (MTJ) that is vertically integrated above or below the magnet. The MTJ will use the magnetostrictive magnet as the soft magnetic layer (or free layer) and a synthetic anti-ferromagnet (SAF) as the hard magnetic layer (or fixed layer) with a tunneling layer in between. Let us assume that the magnetization of the fixed layer is along the direction that encodes bit “1.” Then the MTJ resistances with the soft layer’s magnetization encoding bit “0” and bit “1” will bear a ratio $r = \frac{1+\eta_1\eta_2}{1+\eta_1\eta_2\cos(\Theta)}$, where the η -s are the spin injection/detection efficiencies of the two magnet interfaces of the MTJ and Θ is the angular separation between the two stable magnetization directions in the MTJ’s free layer encoding the two bits. The maximum value of this ratio (assuming $\eta_1 = \eta_2 = 1$) is 2:1 since $\Theta \leq 90^\circ$. Such a low ratio may impair the ability to distinguish between bits “0” and “1” in a noisy environment when the bits are read by measuring the MTJ resistance.

We show that the ratio r can be improved without sacrificing any other metric if we introduce *two* pairs of electrodes (instead of just one) to generate stresses along two *different* directions in the magnet. We will still use a static magnetic field along the minor axis of the ellipse to displace the stable states from the major axis, but this field will be smaller in strength so that the displacement from the major axis is smaller. Consequently, the angular separation

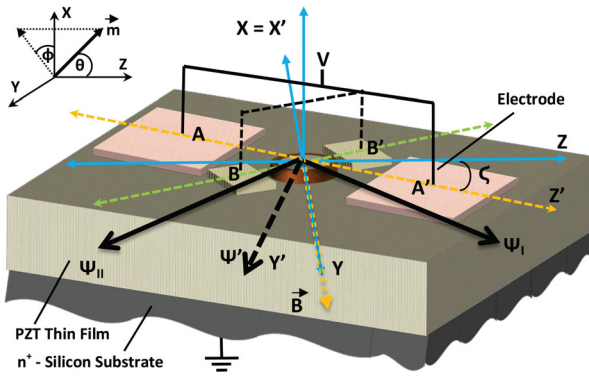


FIG. 1. Schematic illustration of the system with two pairs of electrodes (AA' and BB') and the Terfenol-D nanomagnet delineated on top of a PZT piezoelectric layer. If the magnetization of the Terfenol-D nanomagnet was initially in the stable state Ψ_I (bit “0”), a voltage applied between the electrode pair AA' and ground will switch its direction to the other stable state Ψ_{II} (writing the new bit “1”), while a voltage applied between the pair BB' and ground will keep it in the original stable state Ψ_I (re-writing the old bit “0”). Thus, either bit can be written by activating the correct electrode pair, irrespective of what the initially stored bit was.

between the stable magnetization orientations will be larger ($\Theta > 90^\circ$), resulting in a larger value of r .

Figure 1 shows the schematic of our proposed device. The lead zirconate titanate (PZT) film has a thickness of ~ 100 nm and is deposited on a conducting n^+ -Si substrate. The elliptical nanomagnet has a major axis $a = 110$ nm, minor axis $b = 90$ nm, and thickness $d = 9$ nm. These dimensions ensure that the nanomagnet has a single magnetic domain.¹² One pair of electrode pads has edge dimension of 170 nm and the other has edge dimension of 70 nm. As explained in the supplementary material,¹⁷ these dimensions are needed to ensure the following: (1) the line joining the centers of each pair of pads lies close to one of the stable magnetization orientations, (2) the spacing between the facing edges of the pads in either pair is comparable to the pad's edge dimension and also the PZT film thickness, and (3) no two pads overlap. A small magnetic field ($B = 8.5$ mT) is applied along the in-plane hard axis of the magnet, which brings the magnetization stable states out of the major axis, but retain them in the plane of the magnet ($\phi = \pm 90^\circ$). The new stable states (the two degenerate energy minima) are Ψ_I at $\theta = 24.09^\circ$ and Ψ_{II} at $\theta = 155.9^\circ$, where θ is the angle subtended by the magnetization vector with the z-axis (or major axis of the elliptical magnet). Therefore, the angular separation between these states is $\sim 132^\circ$. The electrodes are delineated such that the line joining one pair subtends an angle $\zeta = 15^\circ$ with the z-axis and the line joining the other pair subtends an angle $\zeta = 165^\circ$. Therefore, the axis joining one pair lies close to one stable magnetization direction and the other lies close to the other stable magnetization direction.

An electrode pair is activated by applying an electrostatic potential between both members of that pair and the grounded substrate. Since the electrode in-plane dimensions are comparable to the piezoelectric film thickness, the out-of-plane (d_{33}) expansion/contraction and the in-plane (d_{31}) contraction/expansion of the piezoelectric regions underneath the electrodes produce a highly localized strain field under the electrodes.¹³ Furthermore, since the electrodes are separated by a distance 1–2 times the PZT film thickness, the interaction between the local strain fields below the electrodes will lead to a biaxial strain in the PZT layer underneath the magnet.¹³ This biaxial strain (compression/tension along the line joining the electrodes and tension/compression along the perpendicular axis) is transferred to the magnet, thus rotating its magnetization. This happens despite any substrate clamping and despite the fact that the electric field in the PZT layer just below the magnet is approximately zero since the metallic magnet shorts out the field.¹³ Activating one pair of electrodes in this fashion moves the magnet's magnetization by $\sim 90^\circ$ away from the axis joining this pair. Upon deactivation (withdrawal of the voltage), the magnetization migrates to the closer stable state with $\geq 99.9998\%$ probability at room temperature and remains there in perpetuity. This writes one bit (say, “0”) in the memory. If we wish to write the other bit (say, “1”), we will activate the other pair of electrodes. Similar to the scheme of Refs. 8–10, this mechanism writes the desired bit with very high reliability ($\geq 99.9998\%$ probability) irrespective of the bit that was stored earlier in the nanomagnet. In the rest of this Letter, we compare our modified scheme with that original scheme of Refs. 8–10 for devices with identical thermal stability factor,¹⁴ static error probability and data retention time at room temperature, and switching time. We show that our scheme not only produces a higher ratio r but is also more energy-efficient and more resilient against dynamic write errors.

We define our coordinate system such that the magnet's easy (major) axis lies along the z-axis and the in-plane hard (minor) axis lies along the y-axis. Uniaxial stress is applied in-plane at an angle ζ from the easy axis because of the disposition of the electrodes. To derive general expressions for the instantaneous potential energies of the nanomagnet due to shape-anisotropy, stress-anisotropy, and the static magnetic field, we rotate our coordinate system such that the z' -axis in the rotated frame coincides with the direction of applied stress. In the following, quantities with a prime are measured in the rotated frame of reference.

Using the rotated coordinate system (see Fig. 1), the shape anisotropy energy of the nanomagnet $E_{sh}(t)$ can be written as

$$\begin{aligned}
 E_{sh}(t) &= E_{s1}(t)\sin^2\theta'(t) + E_{s2}(t)\sin 2\theta'(t) + \frac{\mu_0}{2}\Omega M_s^2(N_{d-yy}\sin^2\zeta + N_{d-zz}\cos^2\zeta), \\
 E_{s1}(t) &= \left(\frac{\mu_0}{2}\right)\Omega M_s^2\{N_{d-xx}\cos^2\phi'(t) + N_{d-yy}\sin^2\phi'(t)\cos^2\zeta - N_{d-yy}\sin^2\zeta + N_{d-zz}\sin^2\phi'(t)\sin^2\zeta - N_{d-zz}\cos^2\zeta\}, \\
 E_{s2}(t) &= \left(\frac{\mu_0}{4}\right)\Omega M_s^2(N_{d-zz} - N_{d-yy})\sin\phi'(t)\sin 2\zeta,
 \end{aligned} \tag{1}$$

where $\theta'(t)$ and $\phi'(t)$ are, respectively, the instantaneous polar and azimuthal angles of the magnetization vector in the rotated frame, M_s is the saturation magnetization of the magnet, N_{d-xx} , N_{d-yy} , and N_{d-zz} are the demagnetization factors that can be evaluated from the nanomagnet's dimensions,¹⁵ μ_0 is the permeability of free space, and $\Omega = (\pi/4)abd$ is the nanomagnet's volume. The potential energy due to the static magnetic flux density B applied along the in-plane hard axis is given by

$$E_m(t) = M_s \Omega B (\cos \theta'(t) \sin \zeta - \sin \theta'(t) \sin \phi'(t) \cos \zeta). \quad (2)$$

When a positive voltage is imposed between the electrode pair AA', it generates either compressive or tensile uniaxial stress in the magnetostrictive nanomagnet depending on the sign of the magnet's magnetostriction coefficient. The stress anisotropy energy is given by

$$E_{str}(t) = -\frac{3}{2} \lambda_s \epsilon(t) Y \Omega \cos^2 \theta'(t), \quad (3)$$

where λ_s is the magnetostriction coefficient, Y is the Young's modulus, and $\epsilon(t)$ is the strain generated by the applied voltage at the instant of time t . The total potential energy of the nanomagnet at any instant t is

$$E(t) = E_{sh}(t) + E_m(t) + E_{str}(t). \quad (4)$$

Figure 2 shows the potential energy profile of the nanomagnet in the magnet's plane ($\phi = 90^\circ$) as a function of the angle θ subtended by the magnetization vector with the major axis of the ellipse (z-axis). When no stress is applied and the static magnetic field is absent (curve I), the energy minima and the stable magnetization states lie along the major axis of the ellipse ($\theta = 0^\circ, 180^\circ$) and the in-plane energy barrier separating them is ~ 145 kT at room temperature. Application of the static magnetic field along the minor axis (curve II) moves the

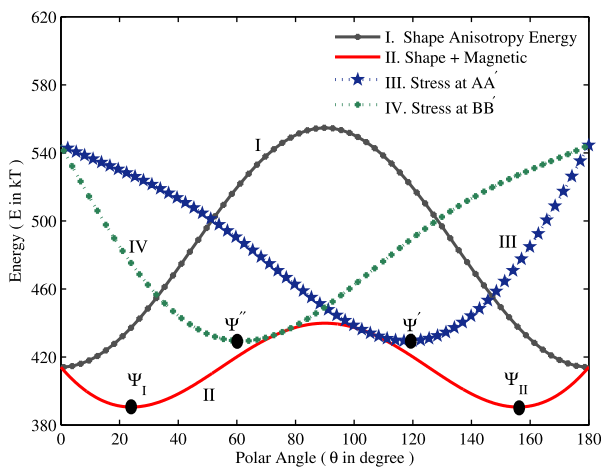


FIG. 2. In-plane potential energy profile (azimuthal angle $\phi = 90^\circ$) of the nanomagnet in different conditions. Curve I shows the profile in the absence of any stress and the static magnetic field, where the energy minima are at $\theta = 0^\circ, 180^\circ$. Curve II shows the profile in the presence of an in-plane magnetic field of 8.5 mT along the nanomagnet's minor axis where the energy minima have moved to $\theta = 24.09^\circ$ and at $\theta = 155.9^\circ$. Curves III and IV show the profile when a compressive stress of 9.2 MPa is generated by imposing a potential between the electrodes AA' and the electrodes BB', respectively. Note that stress makes the potential profile monostable, instead of bistable.

energy minima and stable magnetization states out of the major axis to $\theta = 24.09^\circ$ and 155.9° , while reducing the in-plane energy barrier separating the stable states to 49.2 kT. Therefore, the probability of spontaneous magnetization flipping between the two stable states due to thermal noise (static error probability) is $\sim e^{-49.2}$ per attempt,¹⁴ leading to memory retention time $(1/f_o)e^{-49.2} = 73$ yr, assuming the attempt frequency f_o is 1 THz.¹⁶ The new stable states are designated as Ψ_I (which encodes the binary bit "0") and Ψ_{II} (which encodes the binary bit "1").

Application of sufficient compressive stress along the line joining the electrode pair AA' makes the potential profile monostable (instead of bistable; see curve III) and shifts the minimum energy position to Ψ' , so that the system will go to this state, regardless of whether it was originally at state Ψ_I or Ψ_{II} . After stress removal, the magnetization will end up in the stable state Ψ_{II} (with very high probability at room temperature) since it is the energy minimum closer to Ψ' and getting to Ψ_I from Ψ' would have required transcending the energy barrier between Ψ' and Ψ_I . Thus, activating the pair AA' deterministically writes the bit "1," regardless of the initially stored bit. Similarly, activating the other pair BB' would have written the bit "0" (curve IV of Fig. 2).

In order to calculate the energy dissipated in writing a bit, as well as the probability with which the bit is written correctly in the presence of thermal noise, we have to solve the stochastic Landau-Lifshitz-Gilbert equation. For this, we derive equations for the time evolution of the polar and azimuthal angles of the magnetization vector in the rotated coordinate system (see the accompanying supplementary material¹⁷ for the derivation)

$$\begin{aligned} \frac{d\theta'(t)}{dt} = & -\frac{|\gamma|}{(1+\alpha^2)\mu_0 M_s \Omega} \{E_{\phi 1}(t) \sin \theta'(t) + E_{\phi 2}(t) \cos \theta'(t) \\ & - M_s \Omega B \cos \zeta \cos \phi'(t) - \mu_0 M_s \Omega h_\phi(t) \\ & + \alpha \{E_{s1}(t) \sin 2\theta'(t) - \mu_0 M_s \Omega h_\theta(t) \\ & + 2E_{s2}(t) \cos 2\theta'(t) + (3/2) \lambda_s \epsilon(t) Y \Omega \sin 2\theta'(t) \\ & - M_s \Omega B (\cos \zeta \sin \phi'(t) \cos \theta'(t) + \sin \theta'(t) \sin \zeta)\}, \end{aligned} \quad (5)$$

$$\begin{aligned} \frac{d\phi'(t)}{dt} = & \frac{|\gamma|}{\sin \theta'(t) (1+\alpha^2) \mu_0 M_s \Omega} \{E_{s1}(t) \sin 2\theta'(t) \\ & + 2E_{s2}(t) \cos 2\theta'(t) + (3/2) \lambda_s \epsilon(t) Y \Omega \sin 2\theta'(t) \\ & - M_s \Omega B (\cos \zeta \sin \phi'(t) \cos \theta'(t) + \sin \zeta \sin \theta'(t)) \\ & - \mu_0 M_s \Omega h_\theta(t) - \alpha (E_{\phi 1}(t) \sin \theta'(t) + E_{\phi 2}(t) \cos \theta'(t) \\ & - M_s \Omega B \cos \zeta \cos \phi'(t) - \mu_0 M_s \Omega h_\phi(t))\}. \end{aligned} \quad (6)$$

Solutions of these two equations yield the magnetization orientation $(\theta'(t), \phi'(t))$ at any instant of time t .

In order to generate the stress-induced magnetodynamically in the presence of thermal noise from the last two equations, we need to pick (with appropriate statistical weighting) the initial magnetization state from the thermal distributions around the two stable states Ψ_I and Ψ_{II} in the absence of stress. We determine the thermal distribution around, say, Ψ_I by starting with the initial state $\theta = 24.09^\circ$ and $\phi = 90^\circ$ and solving Eqs. (5) and (6) to obtain the final

values of θ and ϕ by running the simulation for 1 ns while using a time step of $\Delta t = 0.1$ ps (the distributions are verified to be independent of Δt and simulation duration). This procedure is then repeated 10^6 times to obtain the thermal distribution of θ and ϕ around Ψ_I . The same method is employed to find the thermal distribution around Ψ_{II} .

Let us say that we wish to study the (thermally perturbed) stress-induced magnetodynamics associated with writing the bit “1” when the initial stored bit was “0.” We apply a voltage between the electrode pair AA' and the grounded substrate to produce stress in the magnet and generate a switching trajectory by solving Eqs. (5) and (6) after picking (with appropriate statistical weight) the initial orientation from the thermal distribution around Ψ_I ($\theta = 24.09^\circ$ and $\phi = 90^\circ$), which represents the initial bit “0.” After the stress duration is over, the stress is turned off and we continue to simulate the switching trajectory from Eqs. (5) and (6) until the value of θ approaches within 4° of either $\theta = 155.9^\circ$ (correct switching) or $\theta = 24.09^\circ$ (failed switching). The switching time is the minimum time needed for nearly all of the trajectories to switch correctly. It is larger than the stress duration (which is 0.8 ns) and is about 1.5 ns if 99.9998% of the trajectories were to switch correctly. One million switching trajectories are generated and the fraction of them that fail is the dynamic write error probability. If no failure occurs, we conclude that the dynamic error probability is less than 10^{-6} .

We assume the following material parameters for the magnet (Terfenol-D): saturation magnetization $M_s = 8 \times 10^5$ A/m, magnetostriction coefficient $(3/2)\lambda_s = 90 \times 10^{-5}$, Young's modulus $Y = 80$ GPa, and Gilbert damping coefficient $\alpha = 0.1$.^{18–20} We also assume: strain $\epsilon(t) = 1.15 \times 10^{-4}$ (stress = 9.2 MPa) and $\zeta = 15^\circ$.

In Ref. 13, the electric field needed to generate a local strain of $\sim 10^{-3}$ in the magnet was 3 MV/m. Using a linear interpolation, the electric field needed to generate a strain of 1.15×10^{-4} would be 0.345 MV/m. Therefore, the potential that needs to be applied to the electrodes is 0.345 MV/m $\times 100$ nm = 34.5 mV.

The energy dissipated in writing the bit has two components: (1) the *internal* dissipation in the nanomagnet due to Gilbert damping, which is calculated in the manner of Ref. 21 for each trajectory (the mean dissipation is the dissipation averaged over all trajectories that result in correct switching); and (2) the *external* $(1/2) CV^2$ dissipation associated with applying the voltage between the electrodes and the grounded substrate which act as a capacitor. The larger electrode has a lateral dimension of 170 nm and the PZT film thickness is 100 nm. Therefore, the associated capacitance is $C = 2.5$ fF, if we assume that the relative dielectric constant of PZT is 1000. Since the two electrodes of a pair are always activated together, the external energy dissipation will be twice $(1/2) CV^2$ dissipation and that value is 718 kT at room temperature ($V = 34.5$ mV). The smaller electrode pair will have a smaller capacitance and hence dissipate less energy. The mean internal dissipation could depend on whether the initial stored bit was “0” or “1,” and we will take the higher value. In this case, the higher value was 132 kT.

We found that when the initial stored bit is “0,” the bit “1” is written with less than 10^{-6} error probability (not a

single failure among the one million trajectories simulated), while when the initial stored bit is “1,” the bit “1” is written with an error probability of 2×10^{-6} (only two failures among one million trajectories simulated).

Finally, we compare our scheme with that of Refs. 8–10 where compressive or tensile stress is applied at an angle $\zeta = 45^\circ$ with the major axis of the elliptical nanomagnet to write a bit. In this case, the two stable in-plane magnetization directions must correspond to $\theta = \sim 45^\circ$ and $\sim 135^\circ$ (Ref. 9) since they must be close to the stress direction. This would require a higher in-plane static magnetic field since the stable states are to be displaced by a larger angle from the major axis. We would also want the in-plane barrier height separating the two stable states to be the same 49.2 kT at room temperature. We found that these requirements are satisfied if we choose an elliptical nanomagnet of dimensions 150 nm \times 63 nm \times 11 nm and a static magnetic field ($B = 57.3$ mT) along the in-plane hard axis. In this case, the stable states are at $\theta = 46^\circ$ (Ψ_I) and $\theta = 134.5^\circ$ (Ψ_{II}). The angular separation between the two stable directions is 88.5° . In order to get the lowest dynamic error probability in writing a bit, we need to generate a slightly larger strain of 2.4×10^{-4} (stress = 19.5 MPa) by applying a slightly larger voltage (73 mV). We also need to keep the strain on for a slightly longer duration (1.5 ns) to complete writing the bit with least dynamic error probability. With these parameters, we found that the dynamic error probability in writing the bit “1” is 2.1×10^{-5} when the initial bit is “1” (21 failures in 1×10^6 trajectories) and 5×10^{-6} when the initial bit is “0” (5 failures in 1×10^6 trajectories). The switching time is still about 1.5 ns. The average internal dissipation is 295 kT (the dissipation is larger because of the larger stress, larger magnetic field, and longer stress duration needed to achieve the same dynamic error probability) and the external dissipation is 1132 kT if we assume the electrode's edge dimension to be 100 nm (the dissipation is larger because of the larger voltage needed to generate the larger stress). The magnet and other parameters used in Refs. 8–10 were different, but resulted in a much higher energy dissipation of ~ 23 000 kT.¹⁰ We have therefore re-designed their magnet to reduce the energy dissipation significantly. We have also re-designed their electrical scheme to mirror ours because if one applies a potential between the two electrodes of a pair, the resulting electric field will be shorted out directly underneath the magnet, resulting in considerably reduced stress in the magnet.

Table I presents a comparison between the two schemes where we have assumed that the spin injection and detection efficiencies (η_1, η_2) are $\sim 70\%$ at room temperature.²² Clearly, the present scheme is better in all respects.

TABLE I. Comparison between the 2-electrode and 4-electrode schemes.

	2-electrode	4-electrode
Angular separation between stable states (Θ)	88.5°	132°
Static error probability at room temperature	4.29×10^{-22}	4.29×10^{-22}
Dynamic error probability at room temperature	2.1×10^{-5}	2×10^{-6}
Mean switching time (ns)	1.5	1.5
Mean internal energy dissipation (kT)	295	132
External energy dissipation (kT)	1132	718
Mean total energy dissipation (kT)	1427	850
Resistance ratio r	1.47	2.21

In conclusion, we have shown that modifying the scheme of Refs. 8–10 to replace the single pair of electrodes with two pairs imposes a slight additional lithographic burden, but the payoff in terms of energy dissipation, dynamic error rate and resistance ratio more than justifies it. Since the total energy needed to write a bit in the modified scheme is ~ 850 kT, it could be one of the most energy-efficient strategies to write bits in non-volatile magnetic memory. This energy is at least *five orders of magnitude* lower than what has been predicted for spin-transfer-torque memory.²³ Any degradation in the d_{33} coefficient of PZT in a 100-nm thin film²⁴ will of course require a higher writing voltage and hence a higher amount of energy dissipation, but since the dissipation is so low, some degradation will be tolerable.

This work was supported by the U.S. National Science Foundation under Grants. ECCS-1124714 and CCF-1216614. J.A. would also like to acknowledge the NSF CAREER Grant CCF-1253370 and private communication with Professor C. S. Lynch of the Department of Mechanical and Aerospace Engineering at UCLA.

¹M. T. Alam, M. J. Siddiq, G. H. Bernstein, M. T. Niemier, W. Porod, and X. S. Hu, *IEEE Trans. Nanotechnol.* **9**, 348 (2010).

²D. C. Ralph and M. D. Stiles, *J. Magn. Magn. Mater.* **320**, 1190 (2008).

³M. Yamanouchi, D. Chiba, F. Matsukura, and H. Ohno, *Nature* **428**, 539 (2004).

⁴J. Atulasimha and S. Bandyopadhyay, *Appl. Phys. Lett.* **97**, 173105 (2010).

⁵K. Roy, S. Bandyopadhyay, and J. Atulasimha, *Appl. Phys. Lett.* **99**, 063108 (2011).

⁶M. S. Fashami, K. Roy, J. Atulasimha, and S. Bandyopadhyay, *Nanotechnology* **22**, 155201 (2011).

⁷K. Roy, S. Bandyopadhyay, and J. Atulasimha, *Sci. Reports* **3**, 3038 (2013).

⁸N. Tiercelin, Y. Dusch, V. Preobrazhensky, and P. Pernod, *J. Appl. Phys.* **109**, 07D726 (2011).

⁹S. Giordano, Y. Dusch, N. Tiercelin, P. Pernod, and V. Preobrazhensky, *Phys. Rev. B* **85**, 155321 (2012).

¹⁰S. Giordano, Y. Dusch, N. Tiercelin, P. Pernod, and V. Preobrazhensky, *J. Phys. D: Appl. Phys.* **46**, 325002 (2013).

¹¹N. A. Pertsev and H. Kohlstedt, *Appl. Phys. Lett.* **95**, 163503 (2009).

¹²R. P. Cowburn, D. K. Koltsov, A. O. Adeyeye, M. E. Welland, and D. M. Tricker, *Phys. Rev. Lett.* **83**, 1042 (1999).

¹³J. Cui, J. L. Hockel, P. K. Nordeen, D. M. Pisani, C. y. Liang, G. P. Carman, and C. S. Lynch, *Appl. Phys. Lett.* **103**, 232905 (2013).

¹⁴W. F. Brown, Jr., *Phys. Rev.* **130**, 1677 (1963).

¹⁵S. Chikazumi, *Physics of Magnetism* (Wiley New York, 1964).

¹⁶P. Gaunt, *J. Appl. Phys.* **48**, 3470 (1977).

¹⁷See supplementary material at <http://dx.doi.org/10.1063/1.4882276> for explanation of strain generated inside the magnet due to the applied potential at the electrodes.

¹⁸R. Abbundi and A. E. Clark, *IEEE Trans. Magn.* **13**, 1519 (1977).

¹⁹K. Ried, M. Schnell, F. Schatz, M. Hirscher, B. Ludescher, W. Sigle, and H. Kronmüller, *Phys. Status Solidi A* **167**, 195 (1998).

²⁰R. Kellogg and A. Flatau, *J. Intell. Mater. Syst. Struct.* **19**, 583 (2008).

²¹K. Roy, S. Bandyopadhyay, and J. Atulasimha, *J. Appl. Phys.* **112**, 023914 (2012).

²²G. Salis, R. Wang, X. Jiang, R. M. Shelby, S. S. P. Parkin, S. R. Bank, and J. S. Harris, *Appl. Phys. Lett.* **87**, 262503 (2005).

²³K. L. Wang, J. G. Alzate, and P. K. Amiri, *J. Phys. D: Appl. Phys.* **46**, 074003 (2013).

²⁴R. Steinhausen, T. Hauke, W. Seifert, V. Mueller, H. Beige, S. Seifert, and P. Lobmann, in *Proceedings of the Eleventh IEEE International Symposium on Applications of Ferroelectrics, ISAF 98* (1998), pp. 93–96.